HHS Public Access

Author manuscript

Ophthalmic Genet. Author manuscript; available in PMC 2017 December 01.

Published in final edited form as:

Ophthalmic Genet. 2016 December ; 37(4): 445–452. doi:10.3109/13816810.2015.1126616.

Detailed Functional and Structural Phenotype of Bietti Crystalline Dystrophy Associated with Mutations in *CYP4V2* Complicated by Choroidal Neovascularization

Nicole M. Fuerst[1], **Leona Serrano**[1], **Grace Han**[1], **Jessica I. W. Morgan**[1], **Albert M. Maguire**[1,2], **Bart P. Leroy**[2,3,4,5], **Benjamin J. Kim**[1], and **Tomas S. Aleman**[1,2,*]

[1]Scheie Eye Institute and the Perelman Center for Advanced Medicine, University of Pennsylvania, Philadelphia, Pennsylvania

[2] The Division of Ophthalmology of the Children's Hospital of Philadelphia, Department of Ophthalmology, University of Pennsylvania, Philadelphia, Pennsylvania

[3]Center for Cellular & Molecular Therapeutics, the Children's Hospital of Philadelphia, Ghent University and Ghent University Hospital, Belgium.

[4]the Department of Ophthalmology, Ghent University and Ghent University Hospital, Belgium.

[5]Center for Medical Genetics, Ghent University and Ghent University Hospital, Belgium.

Abstract

Purpose—To describe in detail the phenotype of a patient with Bietti crystalline dystrophy (BCD) complicated by choroidal neovascularization (CNV) and the response to intravitreal Bevacizumab (Avastin ®; Genentech/Roche).

Methods—A 34-year-old woman with BCD and mutations in *CYP4V2* (c.802-8_806del13/p.H331P:c992A>C) underwent a complete ophthalmic examination, full-field flash electroretinography (ERG), kinetic and two-color dark-adapted perimetry, and dark-adaptometry. Imaging was performed with spectral domain optical coherence tomography (SD-OCT), near infrared (NIR) and short wavelength (SW) fundus autofluorescence (FAF), and fluorescein angiography (FA).

Results—Best-corrected visual acuity (BCVA) was 20/20 and 20/60 for the right and left eye, respectively. There were corneal paralimbal crystal-like deposits. Kinetic fields were normal in peripheral extent. Retinal crystals were most obvious on NIR-reflectance and corresponded with hyperreflectivities within the RPE on SD-OCT. There was parafoveal/perifoveal hypofluorescence on SW-FAF and NIR-FAF. Rod > cone sensitivity loss surrounded fixation and extended to ~10° of eccentricity corresponding to regions of photoreceptor outer segment-retinal pigmented epithelium (RPE) interdigitation abnormalities. The outer nuclear layer was normal in thickness. Recovery of sensitivity following a ~76% rhodopsin bleach was normal. ERGs were normal. A subretinal hemorrhage in the left eye co-localized with elevation of the RPE on SD-OCT and

*Corresponding author: Tomas S. Aleman, Perelman Center for Advanced Medicine, University of Pennsylvania, 3400 Civic Center Boulevard, Philadelphia, PA 19104. Tel: +1 215 614 4100; Fax: +1 215 615 0527, aleman@mail.med.upenn.edu.

Declaration of Interest: No conflict of interest for any of the authors.

leakage on FA, suggestive of CNV. Three monthly intravitreal injections of Bevacizumab led to restoration of BCVA to baseline (20/25).

Conclusion—Crystals in BCD were predominantly located within the RPE. Photoreceptor outer segment and apical RPE abnormalities underlie the relatively extensive retinal dysfunction observed in relatively early-stage BCD. Intravitreal Bevacizumab was effective in treating CNV in this setting.

Keywords

Bietti crystalline dystrophy; OCT; RPE; CNV; *CYP4V2*

INTRODUCTION

Bietti crystalline dystrophy (BCD) is a rare, autosomal recessive chorioretinal degeneration caused by biallelic mutations in the *CYP4V2* (cytochrome P450 family 4 subfamily V polypeptide 2) gene, a ubiquitously expressed member of the cytochrome p450 protein family involved in the selective hydrolysis of fatty acids. [1, 2] The phenotype of this rare disease has been carefully documented through numerous case reports and case series that date to the pre-molecular era. [3] Clinically, BCD is characterized by a predominantly central retinal degeneration with yellow-white refractile crystals and associated atrophy of the central retinal pigment epithelium (RPE) eventually leading to overt chorioretinal atrophy. [4] A smaller proportion of patients show very small crystals in the superficial corneal stroma. Patients usually present with nyctalopia, decreased visual acuity and constriction of visual fields in their 2nd to 4th decade of life. [5] Despite the reported variability in disease severity, progression to legal blindness and a retina-wide pigmentary retinopathy typically occurs within the next two decades. Choroidal neovascularization (CNV) has only rarely been reported in BCD.[5-11]

Histopathologic reports from patients with BCD are understandably rare, contributing to our incomplete understanding of the pathophysiology of this condition. A recently developed animal model of the disease, the *Cyp4v3*$^{-/-}$ mouse, recapitulates the human phenotype and represents a landmark step forward in the study of the disease. [12] We hereby present a molecularly confirmed (compound heterozygote for two known mutations in *CYP4V2*) patient with BCD complicated by CNV at a relatively early stage of the disease, which permitted a glimpse into the early functional and structural changes, particularly in the setting of this neovascular complication. We used *en face* and cross-sectional retinal imaging in combination with co-localized psychophysical measures of retinal function, which we hope contribute to the current mechanistic hypotheses of this rare condition.

METHODS

A 34-year-old Chinese-American female patient diagnosed with BCD during an eye exam due to floaters and referred for molecular confirmation and further evaluation underwent complete ophthalmic examinations including color fundus photography, fluorescein angiography (FA) and Goldmann kinetic fields. Achromatic (200-ms duration; 1.7° diameter stimuli) and chromatic (500 nm and 650 nm) static perimetry were performed using a

modified Humphrey Field Analyzer (HFA II-*i*, Carl Zeiss Meditec, Dublin, CA), following published methodology. [13] Thresholds were measured along the horizontal meridian at 2° intervals, extending to 30° of eccentricity, corresponding to the retinal region scanned with spectral domain optical coherence tomography (SD-OCT) (see below). Dark-adaptometry was performed using a commercially available instrument (AdaptDx, MacuLogix, Inc., Hummelstown, PA). For this test, pupils were fully dilated and the patient was dark-adapted (>45 min) after which sensitivity was determined with a 505 nm, 200 ms duration, 2° diameter stimulus at 5° in inferior field. Recovery of sensitivity was measured with this stimulus after a localized flash (4° subtend, square area), estimated to isomerize ~76% of rhodopsin, was presented at this location. [14] Psychophysical thresholds were measured every 30 seconds; the test was ended manually when baseline dark-adapted sensitivity was reached. A standard full-field electroretinogram (ERG) was recorded using a computer-based system (Espion, Diagnosys LLC, Littleton, MA). [15] SD-OCT, *en face* near infrared (NIR) reflectance (REF) and fundus autofluorescence (FAF) imaging to NIR and short-wavelength (SW) excitation lights was performed using a Spectralis-HRA system (Heidelberg Engineering GmbH, Heidelberg, Germany). Segmentation of the SD-OCT images was performed with the built-in segmentation software of the Spectralis-HRA system ensuring correct identification of retinal boundaries. [16] Choroidal thickness was measured manually using digital calipers available within the system's software. Comparisons were made with results from normal subjects (n = 42; ages 10-50 years). Informed consent was obtained from all subjects; the procedures adhered to the Declaration of Helsinki and the study was approved by the institutional review board.

RESULTS

The patient had neither a family history of eye disorders nor was there parental consanguinity. Two known compound heterozygote mutations in *CYP4V2* (c. 802-8_806del13 / c.992A>C (p.His331Pro)) were identified; the c.802-8_806del13 mutation was inherited maternally while the c.992A>C (p.His331Pro) mutation was of paternal origin. On initial evaluation, her best-corrected Snellen visual acuity (BCVA) was 20/20 (with a −5.00 D spherical equivalent correction), and 20/30 (−6.00 D), for her right and left eye, respectively. Goldmann visual fields were normal in peripheral extent. The anterior segment examination revealed small paralimbal corneal crystals in both eyes. Fundus examination was significant for the appearance of numerous yellow-white glistening lesions scattered mostly throughout the posterior pole (Fig. 1A). The remainder of the ocular exam was normal. Full-field ERGs were normal for rod-, mixed rod-cone, and cone-mediated responses.

The patient presented six months after her initial evaluation with complaints of distorted central vision in her left eye for two days duration. She denied any other symptoms, including nyctalopia or adaptation complaints. On exam, her BCVA and posterior segment exams were unchanged. SD-OCT showed a thickened hyperreflective band above the Bruch membrane in the temporal parafovea of the left eye (Fig. 1C). FA revealed numerous window defects in both eyes and a localized area of hyperfluorescence temporal to the fovea in the left eye that increased in intensity in later frames, and corresponded to the hyperreflective band on SD-OCT, which was suspicious for CNV (Fig. 1A&C). An

intravitreal anti-vascular endothelial growth factor (anti-VEGF) injection was scheduled, but in the interim, the patient returned in emergency with metamorphopsias and blurred vision. Her left eye BCVA had declined to 20/60 and a small subretinal hemorrhage inferotemporal to the fovea was noted in this eye. She promptly received the first of three monthly intravitreal injections of Bevacizumab in the left eye. At the last follow-up at 4 months, her BCVA had returned to baseline (20/25) with one line improvement from her presenting BCVA but well within the variability of the measurment. [17] She reported nearly resolved metamorphopsia and there was no leakage on FA (Fig. 1 A-C). Follow-up SD-OCT showed a persistent but flattened hyperreflective band without intra- or subretinal hyporeflectivities suggestive of fluid (Fig. 1C).

The question arises as to whether there are features of this patient's phenotype that may be different from other patients with BCD or similar to other genetic retinal degenerations known to be complicated by CNV. This was a unique opportunity to examine in detail the disease expression at a relatively early stage all while following the response to the anti-VEGF treatment. To address this question we evaluated the uncomplicated, uninjected, right eye, after confirming interocular symmetry by SD-OCT (with the exception of the CNV associated abnormalities in the left eye). The yellow-white glistening lesions, commonly described as ‘crystals’, were more numerous in the parafoveal and perifoveal retina, extending into the superior and peripapillary retina (Fig. 2A). These lesions were more evident on NIR-REF. SW-FAF showed an area of mottled hypo-autofluorescence that surrounded the fovea and extended into nasal and superior retina reaching the eccentricity of the vascular arcades (Fig. 2A). Interestingly, NIR-FAF showed a more confluent pattern of hypofluorescence with visualization of the choroidal vasculature virtually throughout the central retina (Fig. 2A). The yellow-white dots were most evident in areas where the FAF signal was the lowest, particularly for the NIR excitation light. There were examples of co-localization of FAF hyperreflective images with the yellow-white dots, but the dots were not discretely autofluorescent to either of the excitation lights. Tenuously hyperautofluorescent dots, however, were noted overlying the choroidal vessels in regions where visualization of the choroidal vasculature was possible through areas of confluent NIR-hypoautofluorescence (Fig. 2A). Horizontal SD-OCT cross sections through the fovea demonstrated a remarkably normal appearance of the nuclear layers. Abnormalities were predominantly observed in structures distal to the photoreceptor inner segment ellipsoid layer. The ellipsoid layer was clearly visible at the foveal center, became non-detectable in the parafovea, and was again discernible only at greater distance from the fovea (>2 mm) in the temporal macula, where the retina showed a more normal lamination and autofluorescence pattern (Fig. 2A & B, *arrows*). The interdigitation of the photoreceptor outer segments and the RPE was not discernible throughout the central retina. There were multiple small hyperreflective dots within the RPE layer, most evident in nasal parafovea, and the choroid appeared thinner compared to normal near the foveal center and in nasal retina.

To understand the consequences that these structural changes have on retinal functioning, SD-OCT thickness parameters were quantified and related to co-localized measures of visual sensitivity. Foveal ONL thickness was within normal limits (122 μm; normal ± 2SD = 112 ± 32 μm), but the distance from the ellipsoid to the RPE layer was reduced to half (25

μm) the normal mean (53 ± 14 μm). Static perimetry showed normal cone-mediated sensitivity at fixation (Fig. 2C, *top panel*), surrounded by paracentral, rod-greater-than-cone, sensitivity losses (Fig. 2C), which co-localized with the ellipsoid and OS-RPE interdigitation abnormalities on SD-OCT. There was a gradual return to better sensitivities with increasing eccentricity from the center coinciding with better appearing retinal lamination. Sensitivity loss was greatest in the nasal parafovea (~2 log units for rod-mediated sensitivity) at 1.2 mm from fixation. At this location, the ONL was normal in thickness (89 μm, normal = 83 ± 22 μm); the OLM was still visible, but the ellipsoid and the OS-RPE interdigitation layers were not discernible. Choroidal thickness in this region was the thinnest (111 μm) compared to normal (253 ± 125μm). Outer retinal layering at an approximately equidistant location from the fovea (1 mm) in temporal retina showed less abnormality. The ellipsoid band was visible although the OS-RPE interdigitation was not discernible. The ONL was normal (97 μm; normal = 86 ± 20 μm) in thickness, but there was a shortened ellipsoid to RPE distance (13 μm) compared to normal (42 ± 8 μm), suggesting outer segment shortening. Choroidal thickness at this location (141 μm) was within normal limits (230 ± 101 μm). The kinetics of recovery of sensitivity following a 76% rhodopsin bleach at a location with ~1 log unit rod sensitivity loss, 1.5 mm in superior retina, was within normal limits (data not shown). Inner retinal laminae were normal in thickness without evidence of retinal remodeling.

To examine the sequence of the structural changes, magnified SD-OCT cross sections from three regions representing different degrees of FAF abnormalities (Fig. 3A, i, ii, iii), were compared with representative normal sections. At the foveal center (Fig. 3A, *i*) there was non-homogeneous hypo-autofluorescence on SW-FAF that extended a greater distance from the center than the hypo-autofluorescence that is normally observed at the fovea (see Fig. 2A, *inset*, for comparison with normal). A better-preserved temporal retina (Fig. 3A, iii) was separated from the hypo-autofluorescent center by a region of patchy hypo- and hyperautofluorescence (Fig. 3A, *ii*). As noted before, the ellipsoid layer was visible at the fovea, the cone OS (COS) length, the distance between the inner segment ellipsoid layer and the apical RPE, was reduced in length and the interdigitation between the COS and the RPE was not discernible. The ellipsoid layer becomes undetectable a short distance from the center where multiple small hyperreflective images were noted within the apical side of the RPE layer, between the ellipsoid and the RPE through a non-discernible OS-RPE interdigitation signal or toward the basal RPE (Fig. 3B, *stars*). In some locations, larger hyperreflective spots were seen extending from the RPE through the external limiting membrane (ELM) into the ONL (Fig. 3B, *arrow*). The greater visibility of the yellow-white dots on *en face* imaging appeared to correspond to this region of absence of the ellipsoid and/or OS-RPE interdigitation signal and hypo-autofluorescence for both excitation wavelengths (Fig. 3 A&B). Examples of round hyperreflective images within the inner retina and deeper than the RPE were observed but were infrequent.

A magnified SD-OCT cross-section from the temporal perifoveal retina (Fig. 3A, *ii*) illustrated possible earlier stages in the development of the abnormalities of the outer retinal sublaminae (Fig. 3C, *left panels*). The temporal side of this section showed a small hyperreflectivity within the apical RPE; a similar lesion nasal to it that fills the hyporeflective gap that normally exists between the OS/RPE-interdigitation layer and the

inner segment ellipsoid layer (Fig. 3C, *white stars*). Nasally, there are no hyperreflective lesions within the RPE but instead a gap in the ellipsoid layer. This finding may explain the disappearance of crystals with disease progression long known to occur in BCD and may signal the onset of more proximal photoreceptor abnormalities (Fig. 3C, *arrow*). [18, 19] Better-preserved retina temporally with less abnormal SW- and NIR-FAF signals showed a near normal retinal lamination with only an occasional hyperreflective lesion within the RPE (Fig. 3C, *right panels, star*).

DISCUSSION

CNV is infrequently reported in association with hereditary retinal degenerations. [20] To our knowledge, ten cases of BCD with CNV have been reported[5-11] with only two in molecularly confirmed *CYP4V2*-associated BCD. [7, 11] If the low prevalence of BCD is taken into account, then the occurrence of CNV in patients with BCD is not uncommon, consistent with a similar observation from a recent BCD case series. [7] Observation of larger groups of patients with BCD in longitudinal, multi-institutional studies will be required to confirm this observation.

The cause of CNV in BCD is not known, although it is likely that breaks in Bruch membrane would be essential for CNV to develop. The opportunity presented, as we were following this patient closely during anti-VEGF therapy, to try to better understand the pathophysiology of this condition, and of the association with CNV, through a detailed phenotypic characterization. *CYP4V2*-associated BCD shows a remarkably consistent phenotype despite reported variability in disease severity. [11, 21-24] In addition to the nearly pathognomonic presence of retinal crystals, other features shared amongst patients include the presence of very fine corneal crystals, nyctalopia and pericentral scotomas with relative preservation of foveal vision and foveal centers reflective of the underlying early regional predilection of the disease to the parafovea/perifovea with extension into the peripapillary and midperipheral retina. [8, 21, 25-31] We found RPE depigmentation on fundus exam limited to the retina immediately nasal to the fovea. SW-FAF and NIR-FAF, on the other hand, revealed more extensive abnormalities including parafoveal and perifoveal hypo-autofluorescence extending nasally and superiorly to the eccentricity of the optic nerve, reminiscent of the pattern reported by ophthalmoscopy, by fluorescein and indocyanine green angiography, and by a few studies using FAF imaging in later stages of the disease. [21, 32-34] The regional predilection suggests vulnerability of this region of high rod and cone photoreceptor cell densities, particularly rods, and of greater photoreceptor-to-RPE cell ratios, a pattern shared by retinal degenerations known to be associated with CNV. [16, 35-39] There was also an extensive loss of the NIR-FAF signal in areas of better preserved SW-FAF, suggesting that RPE depigmentation precedes total outer segment loss and results in accumulation of lipofuscin within RPE cells apposing degenerate photoreceptors. The retinal crystals were seen primarily within the RPE in support of previous observations. Only rarely were crystals observed within the inner retina or deeper to the apical RPE and when this occurred it was typically in regions with severe RPE abnormalities, suggesting displacement. [21, 33, 34, 39-42] There was loss of the photoreceptor outer segment-RPE interface signal on SD-OCT across large expanses of the central retina even in the absence of crystals and in regions where a deceivingly normal ONL co-localized

with abnormal vision. This relative dissociation between the abnormalities at the photoreceptor outer segment-RPE layer in the setting of a preserved ONL lends supports to the hypothesis that these are the structures primarily affected by the molecular defect. [12, 21] Abnormalities of the apical RPE with loss of melanin may also explain the widespread abnormalities observed on NIR-FAF, which were less extensive on SW-FAF. [12] Choroidal thickness was normal in regions of obvious outer segment-RPE change suggesting a sequence where choroidal changes follow RPE and photoreceptor abnormalities.

CYP4V2 encodes a protein highly expressed within RPE cells involved in the degradation of omega-3 polyunsaturated fatty acids, important components of the photoreceptor outer segments. [2] The results support a primary abnormality within the RPE and distal part of the photoreceptor outer segments, perhaps involving the metabolisation of the photoreceptor outer segments or involvement in the homeostasis at the tip of the outer segments/RPE interface, and recapitulates histopathologic findings in a recently developed mouse model of BCD.[12, 21, 43]

In common with other retinal degenerations with CNV associations, particularly AMD and other BCD cases, the abnormalities observed in this patient occurred in the juxtafoveal/parafoveal retina. [44] The regional predilection may relate to the parafoveal disruption of RPE integrity and photoreceptor outer segment-RPE relationships. We demonstrated significant rod sensitivity loss co-localizing to these regions suggestive of a regional predilection for rod dysfunction in early BCD. Retina-wide rod disease demonstrated with full-field ERGs in patients with more advanced disease, elevated dark-adapted thresholds on previous dark-adaptometry measurements, and nyctalopia later in the disease, likely result from the extension of the localized dysfunction to larger expanses of retina. [25, 28, 31, 45-48] Localized cone dysfunction, on the other hand, was less severely affected but was definitely present and likely progressed into absolute scotomas as reported with light-adapted perimetry and multifocal electroretinography. [8, 25, 27, 28, 30, 31, 39, 47, 49-52] It is possible, for example, that the emergence of CNV in BCD may be a consequence of a decline in the production of anti-angiogenic factors by an abnormal RPE subserving high densities of photoreceptors in the foveal and parafoveal retina. [53] The presence of crystals within the RPE may not directly predispose to CNV, since neovascularization would be expected to be much more prevalent, and perhaps, not limited to the fovea and parafovea. It is also possible that CNV only occurs when the RPE fails to maintain the Bruch-RPE-photoreceptor homeostasis, for example as a barrier or source of anti-angiogenic factors in the setting of an otherwise functioning retina, which may explain the observation of CNV in association with locally severe RPE disease and photoreceptor dysfunction. Patients with BCD and CNV have presented during the early stages of the disease, a characteristic shared by our patient and consistent with this idea.[7] Interestingly, CNV complications in retinal degenerations have been most frequently reported in conditions in which there is a closer involvement of the RPE in the pathophysiology, such as Stargardt disease, gyrate atrophy, choroideremia, late-onset retinal degeneration and Best vitelliform dystrophy.[21, 54-58]

Dark adaptation abnormalities have been reported in Sorsby fundus dystrophy, late onset retinal degeneration and AMD, examples of retinal degenerations associated with subretinal neovascularisation as complication. [59, 60] We found no gross recovery abnormalities

following the partial rhodopsin bleach used in this work, supporting a grossly normal function of the retinoid cycle and weighing against primary permeability abnormalities of the RPE-Bruch's membrane thought to both mediate adaptation abnormalities and contribute to the development of CNV in some of the above referenced conditions. [59, 60] Although we tested the rod recovery kinetics at a location with significant rod dysfunction and at a similar distance from the fovea as the region of CNV in the contralateral eye, dark-adaptation abnormalities may still be dependent on local RPE disease severity, and may be only unveiled with greater rhodopsin bleaches or in more advanced disease stages, consistent with a previous report that used full-field bleaches.[47]

Many of the reported cases of CNV in patients with BCD have presented in a similar manner with a small elevated, hyperreflective, juxtafoveal lesion on SD-OCT with associated small subretinal hemorrhage at relatively early disease stages. [6-11] While some reports have shown that CNV can regress without intervention, [5, 6] other studies have reported the success of anti-VEGF agents in CNV associated with BCD. [7, 9, 10] In our patient, in the presence of active CNV and metamorphopsia, anti-VEGF treatment was instituted, resulting in improved visual acuity and decreased visual distortion, supporting the role of the VEGF pathway in the pathophysiology of CNV in BCD and of a role of anti-VEGF therapy in the treatment of CNV in this condition. Awareness of this type of presentation of CNV in these patients may help clinicians diagnose CNV earlier in its course and thus offer earlier treatment.

In conclusion, the detailed phenotypic characterization of this patient with *CYP4V2*-associated BCD supports early primary photoreceptor outer segment - RPE interface abnormalities in this condition. The abnormalities co-localized with changes in the fundus autofluorescence pattern and with localized losses of rod > cone function in the setting of a deceivingly preserved ONL, a pattern uncommon in most primary photoreceptor diseases. Some of these changes may in fact be reversible, which may one day serve as parameters to follow to gauge efficacy of future treatment trials for this condition. The report intends to raise awareness of the possibility of neovascularization even in relatively early-stage BCD and demonstrates the efficacy of anti-VGEF treatment of this complication.

Acknowledgements

Thanks are due to Melissa Eihborn, Sonia Zhu, Jessica Barr and Denise Pearson for their critical help.

Supported by grants from the National Institutes of Health (NEI-K12EY015398-10), Research to Prevent Blindness, Foundation Fighting Blindness, Hope for Vision, Macula Vision Research, the Paul and Evanina Bell Mackall Foundation Trust, The Pennsylvania Lions Sight Conservation and Research Foundation. BPL is a Senior Clinical Investigator of the Research Foundation – Flanders (Belgium) (FWO), and is further supported by FWO Flanders grant OZP 3G004306.

REFERENCES

1. Li A, Jiao X, Munier FL, et al. Bietti crystalline corneoretinal dystrophy is caused by mutations in the novel gene CYP4V2. Am J Hum Genet. 2004; 74(5):817–826. [PubMed: 15042513]
2. Nakano M, Kelly EJ, Wiek C, Hanenberg H, Rettie AE. CYP4V2 in Bietti's crystalline dystrophy: ocular localization, metabolism of omega-3-polyunsaturated fatty acids, and functional deficit of the p.H331P variant. Mol Pharmacol. 2012; 82(4):679–686. [PubMed: 22772592]
3. Mataftsi A, Zografos L, Milla E, Secretan M, Munier FL. Bietti's crystalline corneoretinal dystrophy: a cross-sectional study. Retina. 2004; 24(3):416–426. [PubMed: 15187665]

4. Bietti G. Ueber familiaeres vorkommen von “retinitis punctata albescens” (verbunden mit“dystrophia marginalis cristallinea cormeae”), glitzern des glaskoerpers und anderen degenerativen augenveraenderungen [in German]. Klin Mbl Augenheilk. 1937; 99:737–757.
5. Atmaca LS, Muftuoglu O, Atmaca-Sonmez P. Peripapillary choroidal neovascularization in Bietti crystalline retinopathy. Eye (Lond). 2007; 21(6):839–842. [PubMed: 17173010]
6. Gupta B, Parvizi S, Mohamed MD. Bietti crystalline dystrophy and choroidal neovascularisation. Int Ophthalmol. 2011; 31(1):59–61. [PubMed: 20972604]
7. Li Q, Li Y, Zhang X, et al. Utilization of Fundus Autofluorescence, Spectral Domain Optical Coherence Tomography, and Enhanced Depth Imaging in the Characterization of Bietti Crystalline Dystrophy in Different Stages. Retina. 2015
8. Mamatha G, Umashankar V, Kasinathan N, et al. Molecular screening of the CYP4V2 gene in Bietti crystalline dystrophy that is associated with choroidal neovascularization. Mol Vis. 2011; 17:1970–1977. [PubMed: 21850171]
9. Nachiappan K, Krishnan T, Madhavan J. Ranibizumab for choroidal neovascular membrane in a rare case of Bietti's crystalline dystrophy: a case report. Indian J Ophthalmol. 2012; 60(3):207–209. [PubMed: 22569382]
10. Le Tien V, Atmani K, Querques G, Massamba N, Souied EH. Ranibizumab for subfoveal choroidal neovascularization in Bietti crystalline retinopathy. Eye (Lond). 2010; 24(11):1728–1729. [PubMed: 20798693]
11. Yin H, Jin C, Fang X, et al. Molecular analysis and phenotypic study in 14 Chinese families with Bietti crystalline dystrophy. PLoS One. 2014; 9(4):e94960. [PubMed: 24739949]
12. Lockhart CM, Nakano M, Rettie AE, Kelly EJ. Generation and characterization of a murine model of Bietti crystalline dystrophy. Invest Ophthalmol Vis Sci. 2014; 55(9):5572–5581. [PubMed: 25118264]
13. Jacobson SG, Voigt WJ, Parel JM, et al. Automated light- and dark-adapted perimetry for evaluating retinitis pigmentosa. Ophthalmology. 1986; 93(12):1604–1611. [PubMed: 3808619]
14. Jackson GR, Scott IU, Kim IK, Quillen DA, Iannaccone A, Edwards JG. Diagnostic sensitivity and specificity of dark adaptometry for detection of age-related macular degeneration. Invest Ophthalmol Vis Sci. 2014; 55(3):1427–1431. [PubMed: 24550363]
15. McCulloch DL, Marmor MF, Brigell MG, et al. ISCEV Standard for full-field clinical electroretinography (2015 update). Doc Ophthalmol. 2015; 130(1):1–12.
16. Curcio CA, Messinger JD, Sloan KR, Mitra A, McGwin G, Spaide RF. Human chorioretinal layer thicknesses measured in macula-wide, high-resolution histologic sections. Invest Ophthalmol Vis Sci. 2011; 52(7):3943–3954. [PubMed: 21421869]
17. Arditi A, Cagenello R. On the statistical reliability of letter-chart visual acuity measurements. Invest Ophthalmol Vis Sci. 1993; 34(1):120–129. [PubMed: 8425819]
18. Kaiser-Kupfer MI, Chan CC, Markello TC, et al. Clinical biochemical and pathologic correlations in Bietti's crystalline dystrophy. Am J Ophthalmol. 1994; 118(5):569–582. [PubMed: 7977570]
19. Furusato E, Cameron JD, Chan CC. Evolution of Cellular Inclusions in Bietti's Crystalline Dystrophy. Ophthalmol Eye Dis. 2010; 2010(2):9–15. [PubMed: 21359135]
20. Marano F, Deutman AF, Leys A, Aandekerk AL. Hereditary retinal dystrophies and choroidal neovascularization. Graefes Arch Clin Exp Ophthalmol. 2000; 238(9):760–764. [PubMed: 11045344]
21. Halford S, Liew G, Mackay DS, et al. Detailed phenotypic and genotypic characterization of bietti crystalline dystrophy. Ophthalmology. 2014; 121(6):1174–1184. [PubMed: 24480711]
22. Meng XH, Guo H, Xu HW, et al. Identification of novel CYP4V2 gene mutations in 92 Chinese families with Bietti's crystalline corneoretinal dystrophy. Mol Vis. 2014; 20:1806–1814. [PubMed: 25593508]
23. Lai TY, Ng TK, Tam PO, et al. Genotype phenotype analysis of Bietti's crystalline dystrophy in patients with CYP4V2 mutations. Invest Ophthalmol Vis Sci. 2007; 48(11):5212–5220. [PubMed: 17962476]
24. Astuti GD, Sun V, Bauwens M, et al. Novel insights into the molecular pathogenesis of CYP4V2-associated Bietti's retinal dystrophy. Mol Genet Genomic Med. 2015; 3(1):14–29. [PubMed: 25629076]

25. Bisantis C. G.B. Bietti's sectorial pigmentary retinopathy. Contribution to the knowledge of its various clinical aspects. Ann Ocul (Paris). 1971; 204(9):907–954. [PubMed: 5315629]
26. Yanagi Y, Tamaki Y, Takahashi H, et al. Clinical and functional findings in crystalline retinopathy. Retina. 2004; 24(2):267–274. [PubMed: 15097889]
27. Padhi TR, Kesarwani S, Jalali S. Bietti crystalline retinal dystrophy with subfoveal neurosensory detachment and congenital tortuosity of retinal vessels: case report. Doc Ophthalmol. 2011; 122(3):199–206. [PubMed: 21611771]
28. Liu DN, Liu Y, Meng XH, Yin ZQ. The characterization of functional disturbances in Chinese patients with Bietti's crystalline dystrophy at different fundus stages. Graefes Arch Clin Exp Ophthalmol. 2012; 250(2):191–200. [PubMed: 21892605]
29. Gocho K, Kameya S, Akeo K, et al. High-Resolution Imaging of Patients with Bietti Crystalline Dystrophy with CYP4V2 Mutation. J Ophthalmol. 2014; 2014:283603. [PubMed: 25276414]
30. Parravano M, Sciamanna M, Giorno P, Boninfante A, Varano M. Bietti crystalline dystrophy: a morpho-functional evaluation. Doc Ophthalmol. 2012; 124(1):73–77. [PubMed: 22205354]
31. Sen P, Ray R, Ravi P. Electrophysiological findings in Bietti's crystalline dystrophy. Clin Exp Optom. 2011; 94(3):302–308. [PubMed: 21488952]
32. Lee KY, Koh AH, Aung T, et al. Characterization of Bietti crystalline dystrophy patients with CYP4V2 mutations. Invest Ophthalmol Vis Sci. 2005; 46(10):3812–3816. [PubMed: 16186368]
33. Rossi S, Testa F, Li A, et al. Clinical and genetic features in Italian Bietti crystalline dystrophy patients. Br J Ophthalmol. 2013; 97(2):174–179. [PubMed: 23221965]
34. Kojima H, Otani A, Ogino K, et al. Outer retinal circular structures in patients with Bietti crystalline retinopathy. Br J Ophthalmol. 2012; 96(3):390–393. [PubMed: 21803923]
35. Milam AH, Curcio CA, Cideciyan AV, et al. Dominant late-onset retinal degeneration with regional variation of sub-retinal pigment epithelium deposits, retinal function, and photoreceptor degeneration. Ophthalmology. 2000; 107(12):2256–2266. [PubMed: 11097607]
36. Vincent A, Munier FL, Vandenhoven CC, Wright T, Westall CA, Heon E. The characterization of retinal phenotype in a family with C1QTNF5-related late-onset retinal degeneration. Retina. 2012; 32(8):1643–1651. [PubMed: 22277927]
37. Soumplis V, Sergouniotis PI, Robson AG, et al. Phenotypic findings in C1QTNF5 retinopathy (late-onset retinal degeneration). Acta Ophthalmol. 2013; 91(3):e191–5. [PubMed: 23289492]
38. Jacobson SG, Cideciyan AV, Sumaroka A, Roman AJ, Wright AF. Late-onset retinal degeneration caused by C1QTNF5 mutation: sub-retinal pigment epithelium deposits and visual consequences. JAMA Ophthalmol. 2014; 132(10):1252–1255. [PubMed: 25010528]
39. Gocho K, Kameya S, Akeo K, et al. High-Resolution Imaging of Patients with Bietti Crystalline Dystrophy with CYP4V2 Mutation. J Ophthalmol. 2014; 2014:283603. [PubMed: 25276414]
40. Toto L, Carpineto P, Parodi MB, Di Antonio L, Mastropasqua A, Mastropasqua L. Spectral domain optical coherence tomography and in vivo confocal microscopy imaging of a case of Bietti's crystalline dystrophy. Clin Exp Optom. 2013; 96(1):39–45. [PubMed: 22908902]
41. Manzouri B, Sergouniotis PI, Robson AG, Webster AR, Moore A. Bietti crystalline retinopathy: report of retinal crystal deposition in male adolescent siblings. Arch Ophthalmol. 2012; 130(11): 1470–1473. [PubMed: 23143451]
42. Pennesi ME, Weleber RG. High-resolution optical coherence tomography shows new aspects of Bietti crystalline retinopathy. Retina. 2010; 30(3):531–532. [PubMed: 20139800]
43. Kennedy CJ, Rakoczy PE, Constable IJ. Lipofuscin of the retinal pigment epithelium: a review. Eye (Lond). 1995; 9(Pt 6):763–771. Pt 6. [PubMed: 8849547]
44. Owsley C, Jackson GR, Cideciyan AV, et al. Psychophysical evidence for rod vulnerability in age-related macular degeneration. Invest Ophthalmol Vis Sci. 2000; 41(1):267–273. [PubMed: 10634630]
45. Usui T, Tanimoto N, Takagi M, Hasegawa S, Abe H. Rod and cone a-waves in three cases of Bietti crystalline chorioretinal dystrophy. Am J Ophthalmol. 2001; 132(3):395–402. [PubMed: 11530054]
46. Meng XH, Guo H, Xu HW, et al. Identification of novel CYP4V2 gene mutations in 92 Chinese families with Bietti's crystalline corneoretinal dystrophy. Mol Vis. 2014; 20:1806–1814. [PubMed: 25593508]

47. Wilson DJ, Weleber RG, Klein ML, Welch RB, Green WR. Bietti's crystalline dystrophy. A clinicopathologic correlative study. Arch Ophthalmol. 1989; 107(2):213–221. [PubMed: 2783846]
48. Lin J, Nishiguchi KM, Nakamura M, Dryja TP, Berson EL, Miyake Y. Recessive mutations in the CYP4V2 gene in East Asian and Middle Eastern patients with Bietti crystalline corneoretinal dystrophy. J Med Genet. 2005; 42(6):e38. [PubMed: 15937078]
49. Jiang L, Wen F, Wu L, Yan H, Hu S. Indocyanine green angiographic and multifocal electroretinographic features in the diffuse and regional form of Bietti's crystalline retinopathy. Yan Ke Xue Bao. 2002; 18(1):9–13. [PubMed: 15510667]
50. Gekka T, Hayashi T, Takeuchi T, Goto-Omoto S, Kitahara K. CYP4V2 mutations in two Japanese patients with Bietti's crystalline dystrophy. Ophthalmic Res. 2005; 37(5):262–269. [PubMed: 16088246]
51. Jin ZB, Ito S, Saito Y, Inoue Y, Yanagi Y, Nao-i N. Clinical and molecular findings in three Japanese patients with crystalline retinopathy. Jpn J Ophthalmol. 2006; 50(5):426–431. [PubMed: 17013694]
52. Takikawa C, Miyake Y, Yamamoto S. Re-evaluation of crystalline retinopathy based on corneal findings. Folia Ophthalmol Jpn. 1992; 43:969–978.
53. Glaser BM, Campochiaro PA, Davis JL Jr, Jerdan JA. Retinal pigment epithelial cells release inhibitors of neovascularization. Ophthalmology. 1987; 94(7):780–784. [PubMed: 2443889]
54. Marano F, Deutman AF, Leys A, Aandekerk AL. Hereditary retinal dystrophies and choroidal neovascularization. Graefes Arch Clin Exp Ophthalmol. 2000; 238(9):760–764. [PubMed: 11045344]
55. Palejwala NV, Lauer AK, Weleber RG. Choroideremia associated with choroidal neovascularization treated with intravitreal bevacizumab. Clin Ophthalmol. 2014; 8:1675–1679. [PubMed: 25214760]
56. Battaglia Parodi M, De Benedetto U, Knutsson KA, et al. Juxtafoveal choroidal neovascularization associated with retinitis pigmentosa treated with intravitreal bevacizumab. J Ocul Pharmacol Ther. 2012; 28(2):202–204. [PubMed: 22149640]
57. Campos-Pavon J, Torres-Pena JL. Choroidal neovascularization secondary to choroideremia. Arch Soc Esp Oftalmol. 2015; 90(6):289–291. [PubMed: 25433417]
58. Cheng JY, Adrian KH. Photodynamic therapy for choroidal neovascularization in stargardt disease and retinitis pigmentosa. Retin Cases Brief Rep. 2009; 3(4):388–390. [PubMed: 25389856]
59. Jacobson SG, Cideciyan AV, Wright E, Wright AF. Phenotypic marker for early disease detection in dominant late-onset retinal degeneration. Invest Ophthalmol Vis Sci. 2001; 42(8):1882–1890. [PubMed: 11431457]
60. Steinmetz RL, Haimovici R, Jubb C, Fitzke FW, Bird AC. Symptomatic abnormalities of dark adaptation in patients with age-related Bruch's membrane change. Br J Ophthalmol. 1993; 77(9): 549–554. [PubMed: 8218049]
61. Spaide RF, Curcio CA. Anatomical correlates to the bands seen in the outer retina by optical coherence tomography: literature review and model. Retina. 2011; 31(8):1609–1619. [PubMed: 21844839]

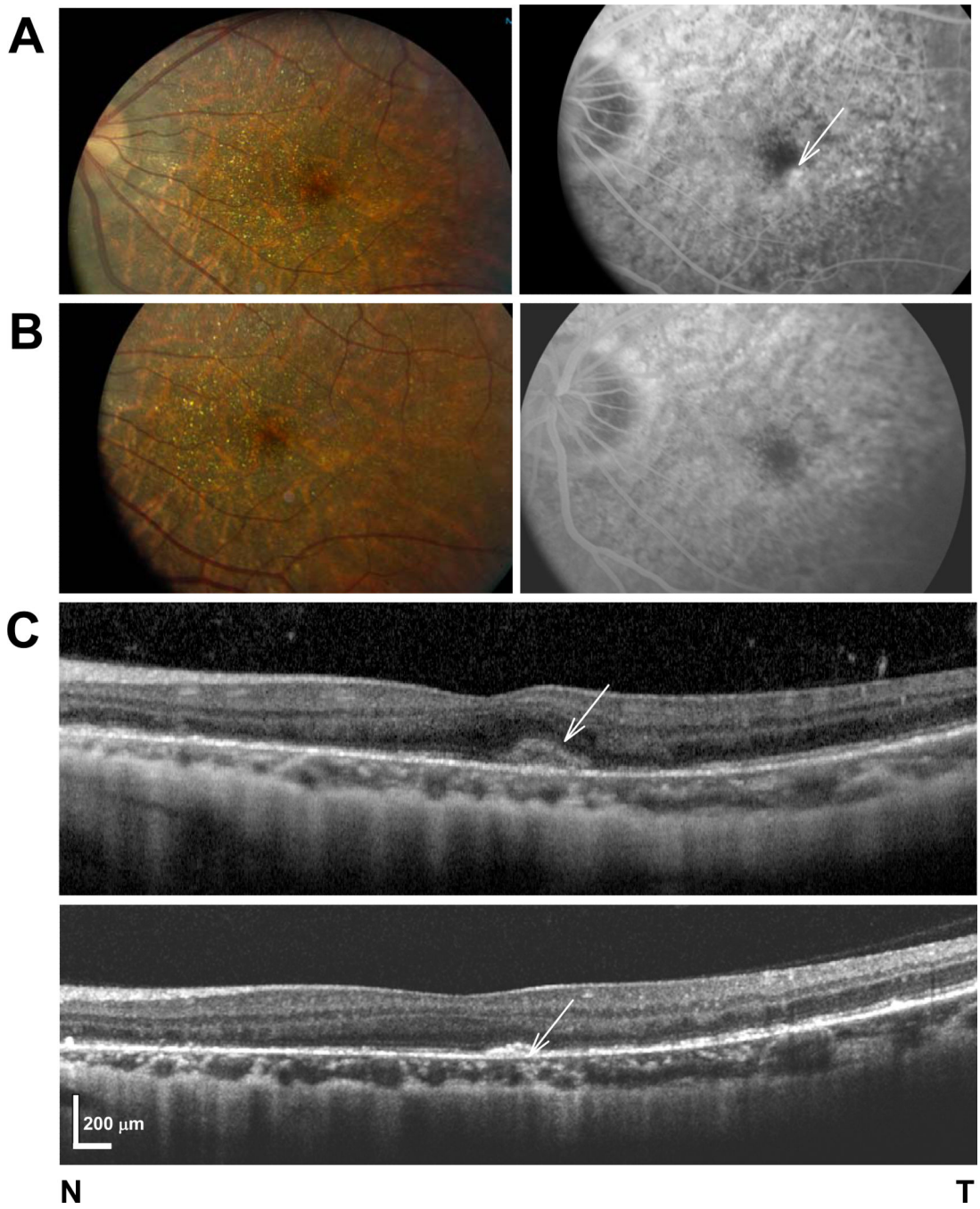

FIGURE 1.

(**A,B)** Fundus photography (*left panel*) and late phase FA (*right panel*) in the patient before (A) and after (B) anti-VEGF therapy. **(C)** SD-OCT horizontal cross-section through the fovea of the symptomatic left eye of the patient before (*top panel*) and after (*bottom panel*) three monthly intravitreal injections of Bevacizumab.

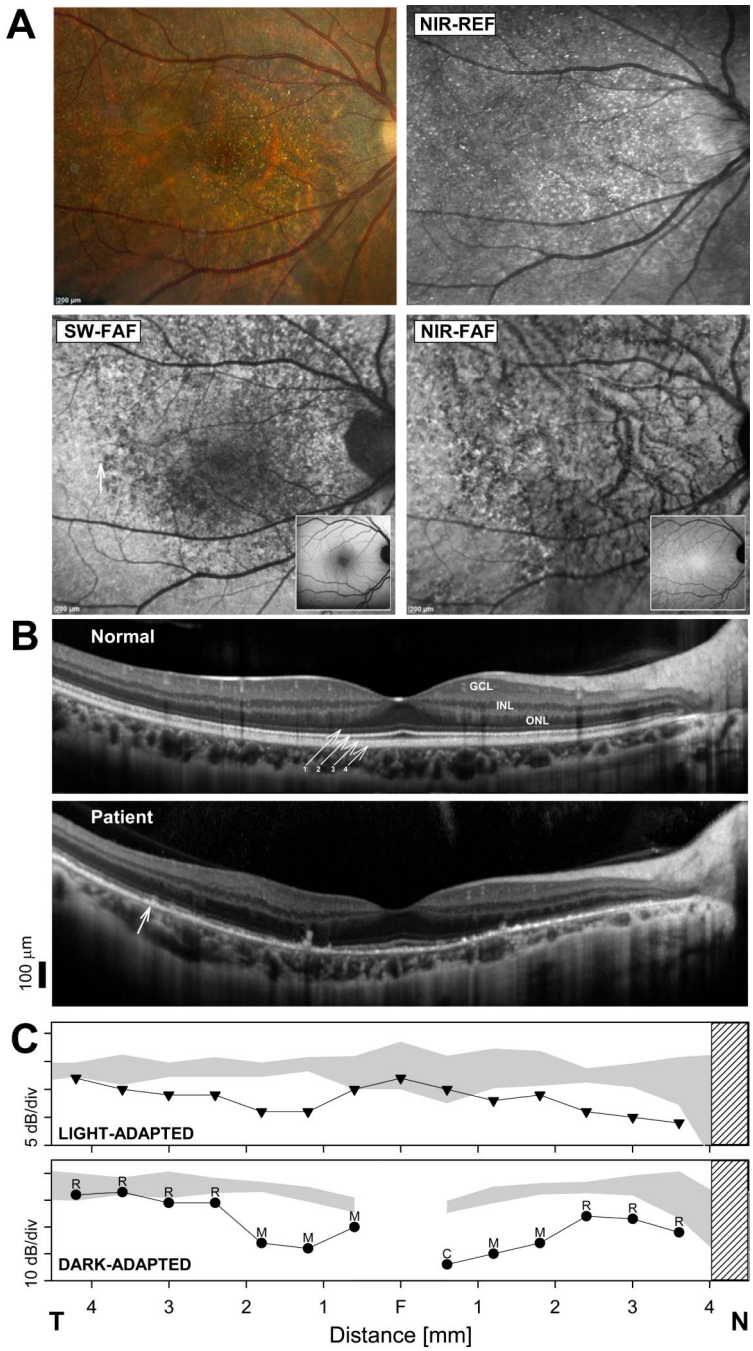

FIGURE 2.

(A) Fundus photography, fundus reflectance and autofluorescence imaging in the patient. Normal appearance of SW-FAF and NIR-FAF imaging are shown as insets. **(B)** SD-OCT horizontal, 9 mm cross sections through the fovea of the patient compared to a representative normal subject. Nuclear layers are labeled: outer nuclear layer = ONL, inner nuclear layer = INL, ganglion cell layer = GCL. Outer retinal layers are labeled (*diagonal arrows*) according to recently proposed nomenclature. [61] 1. OLM, 2. Ellipsoid, 3. Photoreceptor outer segment/RPE interdigitation, 4. RPE. Vertical arrow in the patient denotes boundary region

where the retina transitions from a near normal appearance on FAF imaging in temporal (T) retina to a clearly abnormal signal nasally (N). **(C)** Horizontal sensitivity profiles measured with achromatic, light-adapted (*top panel*), and dark-adapted, chromatic (500 nm), automatic static perimetry in the patient compared to the normal range (g*ray band* = mean ± 2SD). Dark adapted photoreceptor mediation estimated with two color (500 nm and 650 nm) dark adapted perimetry is shown above the dark-adapted sensitivity profile (R = rod; M = mixed cone-rod; C = cone mediation). Gap in the dark-adapted, rod-mediated sensitivity profile corresponds to the rod free region near fixation. *Hatched bar:* blind spot.

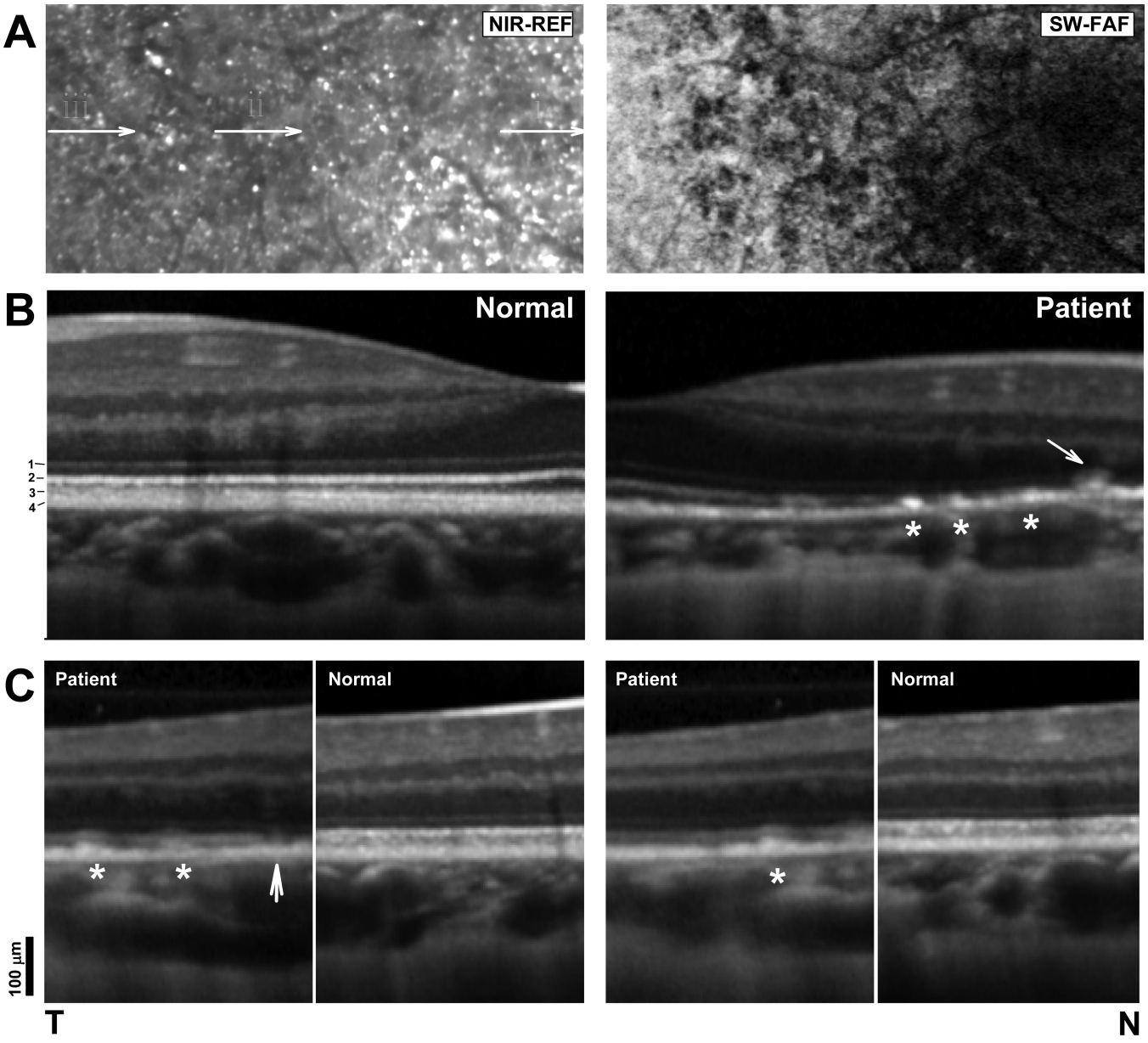

FIGURE 3.

(A) Magnified NIR-REF and SW-FAF from the patient. Arrows in the NIR-REF image denote regions sampled with SD-OCT and orientation of the magnified (B) cross-sections. **(B)** Magnified SD-OCT horizontal cross-section through the fovea into nasal retina in the patient compared with a normal subject. Scans are split at the fovea and flipped horizontally in the normal subject to facilitate comparisons of the details of the outer retinal lamination. Scans are vertically aligned by the RPE/Bruch's layers **(C)** Magnified SD-OCT scans from regions ‘ii’ (left panel) and ‘i’ (right panel) compared with sections from a normal subject. Stars denote RPE hyperreflectivities that correspond to yellow-white dots; arrow points to gap in the ellipsoid layer.